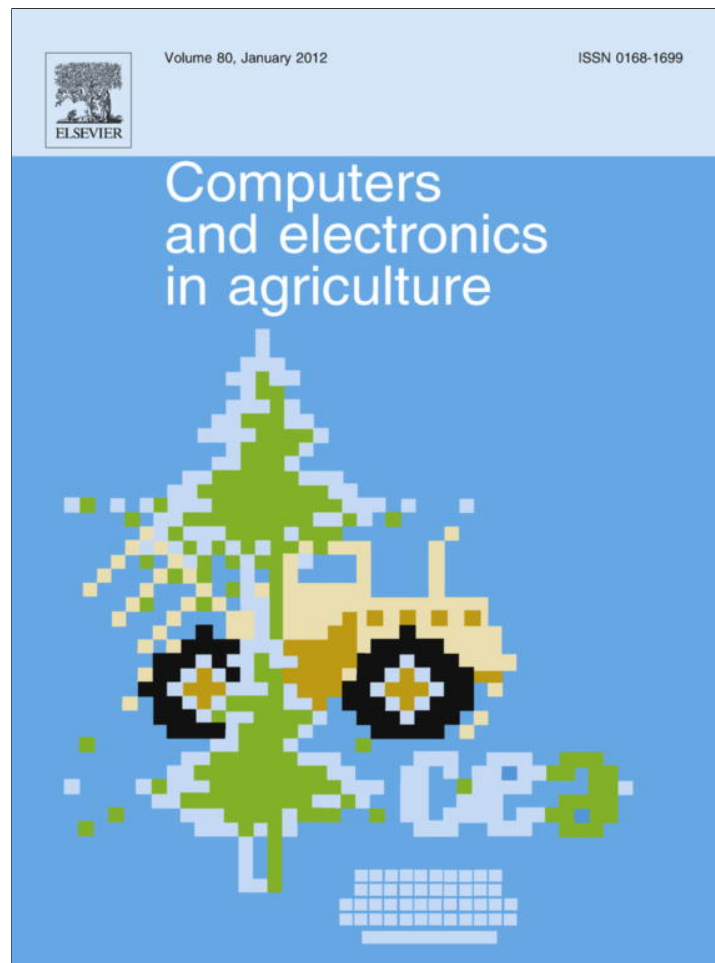


Provided for non-commercial research and education use.
Not for reproduction, distribution or commercial use.



(This is a sample cover image for this issue. The actual cover is not yet available at this time.)

This article appeared in a journal published by Elsevier. The attached copy is furnished to the author for internal non-commercial research and education use, including for instruction at the authors institution and sharing with colleagues.

Other uses, including reproduction and distribution, or selling or licensing copies, or posting to personal, institutional or third party websites are prohibited.

In most cases authors are permitted to post their version of the article (e.g. in Word or Tex form) to their personal website or institutional repository. Authors requiring further information regarding Elsevier's archiving and manuscript policies are encouraged to visit:

<http://www.elsevier.com/copyright>

Contents lists available at [SciVerse ScienceDirect](http://www.sciencedirect.com)

Computers and Electronics in Agriculture

journal homepage: www.elsevier.com/locate/compag

Detecting powdery mildew of winter wheat using leaf level hyperspectral measurements

Jing-Cheng Zhang^{a,b,c}, Rui-liang Pu^b, Ji-hua Wang^a, Wen-jiang Huang^{a,*}, Lin Yuan^{a,c}, Ju-hua Luo^a^a Beijing Research Center for Information Technology in Agriculture, Beijing, China^b Department of Geography, Environment and Planning, University of South Florida, Tampa, FL, USA^c Institute of Agriculture Remote Sensing and Information System Application, Zhejiang University, Hangzhou 310029, China

ARTICLE INFO

Article history:

Received 30 June 2011

Received in revised form 11 February 2012

Accepted 11 March 2012

Keywords:

Powdery mildew

Spectral feature

Partial least square regression (PLSR)

Fisher linear discriminant analysis (FLDA)

Cross validation

ABSTRACT

Powdery mildew (*Blumeria graminis*) is one of the most destructive diseases, which has a significant impact on the production of winter wheat. Detecting powdery mildew via spectral measurement and analysis is a possible alternative to traditional methods in obtaining the spatial distribution information of the disease. In this study, hyperspectral reflectances of normal and powdery mildew infected leaves were measured with a spectroradiometer in a laboratory. A total of 32 spectral features (SFs) were extracted from the lab spectra and examined through a correlation analysis and an independent *t*-test associated with the disease severity. Two regression models: multivariate linear regression (MLR) and partial least square regression (PLSR) were developed for estimating the disease severity of powdery mildew. In addition, the fisher linear discriminant analysis (FLDA) was also adopted for discriminating the three healthy levels (normal, slightly-damaged and heavily-damaged) of powdery mildew with the extracted SFs. The experimental results indicated that (1) most SFs showed a clear response to powdery mildew; (2) for estimating the disease severity with SFs, the PLSR model outperformed the MLR model, with a relative root mean square error (RMSE) of 0.23 and a coefficient of determination (R^2) of 0.80 when using seven components; (3) for discrimination analysis, a higher accuracy was produced for the heavily-damaged leaves by FLDA with both producer's and user's accuracies over 90%; (4) the selected broadband SFs revealed a great potential in estimating the disease severity and discriminating severity levels. The results imply that multispectral remote sensing is a cost effective method in the detection and mapping of powdery mildew.

© 2012 Elsevier B.V. All rights reserved.

1. Introduction

At least 10% of global food production is lost due to plant disease (Christou and Twyman, 2004; Strange and Scott, 2005). Powdery mildew, caused by *Blumeria graminis*, is one of the most widely destructive plant diseases in the world (Reuveni and Reuveni, 1998; Olsen et al., 2003; Nofal and Haggag, 2006). The disease affects a wide range of commercial crops, and can result in a significant yield loss (Sharma et al., 2004; Strange and Scott, 2005). Therefore people have paid a great attention to the impact of powdery mildew on food security (Hardwick et al., 1994). Several studies have addressed the influencing mechanism of powdery mildew from physiological or genetic perspectives, attempting to breed varieties with strong resistance to powdery mildew or to develop effective fungicides (Gooding et al., 1994; Wright et al., 1995; Hu et al., 2008). Meanwhile, great progresses were achieved in pre-

venting and controlling powdery mildew in wheat planted areas. For example, Hardwick et al. (1994) found that a fungicide with fenpropidin and fenpropimorph appeared to be effective in controlling the powdery mildew. Jørgensen and Olesen (2002) discovered that the infection of powdery mildew can be successfully prevented with fungicides containing ergosterol biosynthesis inhibitors. However, although the application of fungicides is effective in controlling the powdery mildew, it is impossible to eradicate the disease at a regional scale since many species of plants can host this pathogen (Eichmann and Hüchelhoven, 2008). Therefore, it is important in practice for crop managers to obtain information about the spatial distribution of powdery mildew in time to guide the spray of fungicide. In addition, an inaccurate application of fungicide can lead to missing infected areas or overuse, especially when using automatic spray systems such as tractors or aircraft.

To obtain the information of disease infected boundaries in the field, the most common and conventional way is conducting a field survey. The traditionally ground-based survey method is very expensive and inefficient and, therefore, is problematic over large

* Corresponding author. Tel.: +86 10 51503647.

E-mail addresses: zjc19840222@gmail.com, yellowstar0618@163.com (W.-j. Huang).

areas. However, remote sensing technology may be a possible alternative for obtaining the spatial distribution information of powdery mildew over a large area with a relatively low cost.

During the last two decades, several studies were successfully conducted to detect crop diseases by means of remote sensing techniques (e.g. West et al., 2003; Sankaran et al., 2010). As stated by Sankaran et al. (2010), optical remote sensing, particularly using spectral features (SFs) extracted from visible and near-infrared (NIR) regions, has great potential in plant disease diagnosis and detection. For example, by using multispectral data, Franke and Menz (2007) successfully detected powdery mildew and leaf rust in a winter wheat field by using normalized difference vegetation index (NDVI). Qin and Zhang (2005) obtained the infected area information of rice sheath blight with broadband high spatial-resolution data. In addition, some researchers have applied hyperspectral remote sensing technique to detection and mapping crop disease. Bravo et al. (2003) and Moshou et al. (2004) developed a ground-based real-time remote sensing system for disease detection in winter wheat field, which achieved a classification accuracy of over 90%. Huang et al. (2007) found that the Photochemical Reflectance Index (PRI) had a strong estimating power for yellow rust disease in winter wheat at canopy level. In their study, a relationship between PRI and disease severity of yellow rust in winter wheat was further confirmed with airborne hyperspectral data. Liu et al. (2010) also used hyperspectral reflectance measurements to make an accurate discrimination of rice fungal diseases at different severity levels. Based on the literature review, it is apparent that the hyperspectral remote sensing has shown an even greater potential in identifying and detecting crop diseases. Hyperspectral remote sensing refers to a special type of imaging technology that collects image data in many narrow contiguous spectral bands (<10 nm band width) throughout the visible and solar-reflected infrared portions of the spectrum (Goetz et al., 1985). Given the fact that various symptoms and the corresponding spectral responses may vary with the diseases, it is thereby necessary to conduct an independent examination on the performance of several commonly used SFs in detecting powdery mildew.

The infection caused by powdery mildew usually leads to a contiguous stretched distribution pattern in the field, which thus provides a good chance for remote sensing applications (Lorenzen and Jensen, 1989). Moreover, the most distinct symptom of powdery mildew of winter wheat is that pustules in light white (sometimes light yellow) color appear on leaves (Rémus-Borel et al., 2005). The portion of pustules on leaves will increase with the severity level, which leads to a significant spectral difference between normal leaves and infected ones, allowing the disease to be detected based on spectral signatures (Jones et al., 2010).

To date, there are a few studies addressing powdery mildew detection using spectral discrimination. The knowledge about the spectral responses to powdery mildew in winter wheat is still lacking. Lorenzen and Jensen (1989) reported the spectral characteristics of powdery mildew in barley. Rumpf et al. (2010) differentiated between diseases *Cercospora* leaf spot, leaf rust and powdery mildew for sugar beet at leaf level by using hyperspectral data. However, none of them has systematically explored the spectral responses that are induced by powdery mildew. In their studies, instead of using extracted SFs, the entire reflectance spectral bands were utilized with some statistical analysis methods to improve estimated accuracy, which would inevitably increase the computational load. The pivotal question, at what severity level can powdery mildew be detected, has not been answered yet. Therefore, the objectives of this study are: (1) To examine responses of a set of possible SFs to powdery mildew in winter wheat at a leaf level, and identify the most suitable SFs for disease detection; (2) to develop multivariate models in estimating the disease severity at a leaf level; and (3) to determine the severity

level of powdery mildew that could be identified with an acceptable accuracy by means of a spectral discrimination analysis.

2. Materials and methods

2.1. Study site and materials

The winter wheat (*Triticum aestivum* L.) plants were grown in an experimental field in Beijing Academy of Agriculture and Forestry Sciences, China, which was located at 39°56'N, 116°16'E at an altitude of 56 m (Fig. 1). Cultivar 'Jingdong 8' was chosen, as it was widely grown in Beijing and Hebei province and is moderately susceptible to powdery mildew. During the months of May and June, 2010, the powdery mildew (*B. graminis*) occurred naturally in approximately a half of the experimental field. The symptoms of powdery mildew were unobvious at early growing stages, however, after the booting stage symptoms developed rapidly, and were visible by the filling stage. Based on the work of Cao et al. (2009), the early period of filling stage is an important time point for conducting preventive procedures such as fungicide spray. Therefore, we conducted the experiment on May 23, 2010 when the filling stage began.

2.2. Data acquisition

2.2.1. Leaf sampling

Leaves were cut from the winter wheat plants in the field with scissors, and samples were packed with ice bags and transported to a nearby indoor laboratory for spectral measurements. Each leaf sample was placed in individual small plastic bags in order to prevent a water loss and cross contamination. There were a total of 114 leaf samples collected for measurement, including 34 normal leaves and 80 diseased leaves with varied severity. Each leaf was wrapped in moistened paper towels right after the spectral measurement, so as to conduct subsequent leaf biochemical analysis.

2.2.2. Leaf spectra and pigment measurement

Leaf reflectance spectra were measured by using a FieldSpec® UV/VNIR spectroradiometer (ASD Inc., Boulder, Colorado, USA) over the 350–1050 nm wavelength range at 3 nm intervals, coupled with a Li-1800 integrating sphere (Li-Cor Inc., Lincoln, Nebraska, USA) as an illumination source. In order to avoid bands with low signal-to-noise ratio at both ends, only the spectra ranging from 450 to 950 nm were retained and applied for subsequent analysis. The spectrum of a white Spectralon reference panel (99% reflectance) was recorded once for every 10 measurements. Leaf reflectance was determined by calculating a ratio of the sample radiance to that of the white Spectralon reference panel. Depending on the heterogeneity of the pustule distributed pattern on the leaf, 10–15 readings were recorded for each leaf, which were then averaged to obtain a spectral measurement for the leaf (sample). Right after spectral measurements, the leaves were cut into pieces and placed in a tube with 10 ml acetone (80%). The pigments were extracted by placing the tube in a 65 °C water tub in a dark room for more than 5 h. Then, concentrations of chlorophyll-*a* (Chl_a), chlorophyll-*b* (Chl_b) and carotenoids (Car) were extracted and computed using the equations of Lichtenthaler (1987) as follows:

$$C_A = 12.25OD_{663} - 2.79OD_{647} \quad (1)$$

$$C_B = 21.50OD_{647} - 5.10OD_{663} \quad (2)$$

$$C_C \text{ (mg/L)} = (1000OD_{470} - 1.82C_A - 85.02C_B)/198 \quad (3)$$

where C_A , C_B , and C_C are concentrations of Chl_a, Chl_b and Car in mgL^{-1} , respectively. OD_{447} , OD_{670} , and OD_{663} are absorbency at specific wavelengths.

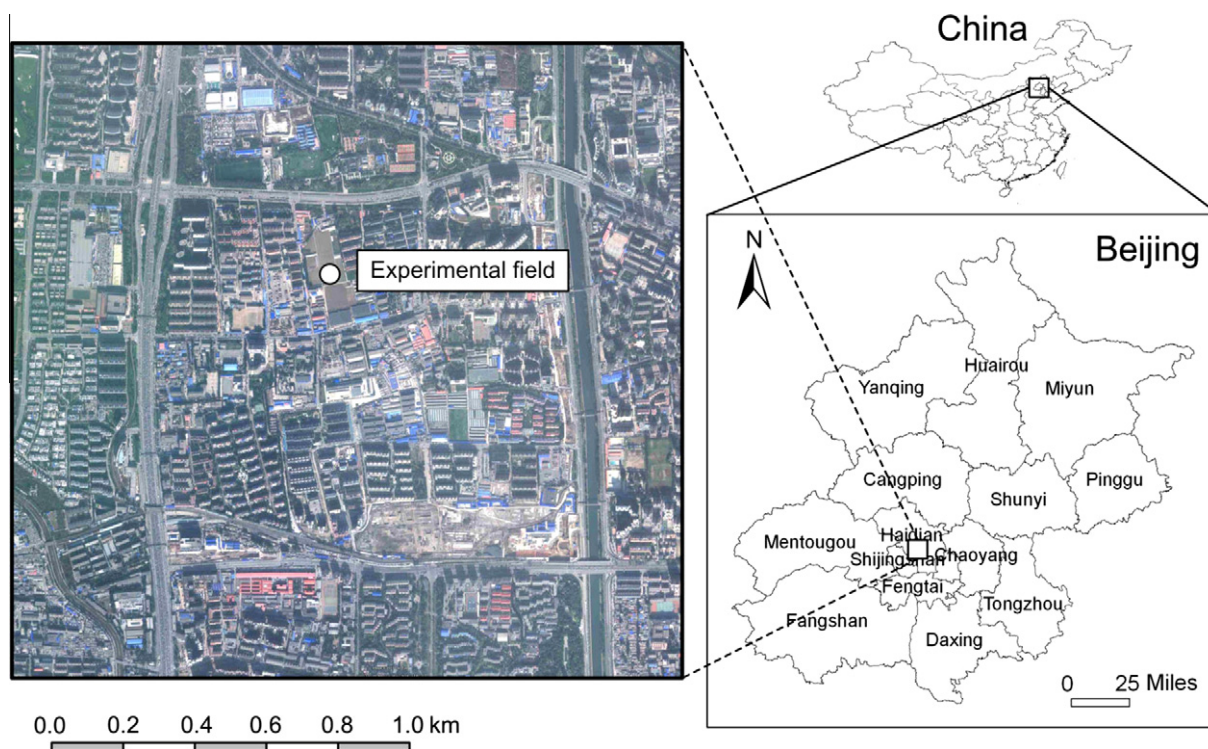


Fig. 1. Location of the experimental field.

2.2.3. Determination of disease severity

The disease severity of each sample was determined by visual estimation of a percentage of an infected leaf surface area based on a color photo, which was taken right after the spectral measurement for each diseased leaf with a background of a white paper following the methods of Graeff et al. (2006) and Luedeling et al. (2009). To further minimize possible error sources that might be incurred by an investigator, the estimated damage percentage was classified into nine classes: 0–3% (no disease), 3–10% (disease index, DI = 1), 11–20% (DI = 2), 21–30% (DI = 3), 31–40% (DI = 4), 41–50% (DI = 5), 51–60% (DI = 6), 61–70% (DI = 7), >70% (DI = 8). In fact, there were no leaves/samples in this experiment with an infected cover percentage higher than 80%, whereas those leaves with a pustule portion less than 3% were actually difficult to visually separate from normal leaves. It should be noted that with this criterion, DI was used as a continuous variable in subsequent regression analysis. Apart from using DI, the disease severity of leaves was also qualitatively categorized by two discrete levels: Slightly-damaged leaves (those leaves with a portion of pustule ranging from 3% to 30%) and heavily-damaged leaves (those leaves with a portion over 30%). The definition of the severity levels of infection referred to the criterion used by the plant protection department (Chinese Standard: NY/T 613-2002). Using these categories, the entire dataset could be reorganized into 3 discrete levels so that a subsequent discrimination analysis could be conducted.

2.3. Selection of SFs

From a physiological perspective, changes of pigment content, cellular structure and appearance of mildew on leaf surface induced by powdery mildew are responsible for the corresponding spectral changes. To utilize those important spectral features potentially sensitive to the changes, a total of 32 spectral features (SFs) were adopted, including nine derivative spectra, three continuous removal transformed parameters, nine broad-band SFs and 11 hyperspectral vegetation indices (VIs, Table 1). Derivative

spectra and continuous removal transformed SFs were used for extracting the spectral characteristics around blue edge, yellow edge, and red edge, which are closely related to the physiological status of plants (Gong et al., 2002; Pu et al., 2003, 2004). Eleven hyperspectral VIs were selected because they either have been used for disease detection, such as Nitrogen Reflectance Index (NRI), Photochemical Reflectance Index (PRI) and Transformed Chlorophyll Absorption and Reflectance Index (TCARI) (Gamon et al., 1992; Filella et al., 1995; Haboudane et al., 2004) or have a potential in detecting stress, such as Red-edge Vegetation Stress Index (RVSI) and Plant Senescence Reflectance Index (PSRI) (Merton and Huntington, 1999; Merzlyak et al., 1999). In addition, the nine broad-band SFs were selected for examining their potential in detecting powdery mildew because they are frequently used for mapping or retrieving vegetation status. Of those, the original band reflectances of green and red bands (based on the wavelength range of Landsat-5 TM) were included for reflecting the color change induced by the lesions caused by powdery mildew. Several other broad-band VIs, such as Simple Ratio (SR), NDVI and Green Normalized Difference Vegetation Index (GNDVI) were also included as they were already used for detecting plant diseases (Zhao et al., 2004; Yang et al., 2007). The band setting of the most common multispectral satellite data – Landsat-5 TM was used for generating the broad-band reflectance. The reflectances of Landsat-5 TM bands were obtained by integrating original hyperspectral reflectances within individual TM band wavelengths with their corresponding relative spectral response (RSR) functions. The integration was done by:

$$R_{\text{broad}} = \int_{b_{\text{high}}}^{b_{\text{low}}} f(x) dx \quad (4)$$

where R_{broad} is the simulated reflectance for a broad-band; b_{low} and b_{high} indicate the low and high limits of the broad-band wavelength. The definitions, descriptions or formulas, and reference sources for all 32 SFs were summarized in Table 1.

Table 1
A summary of a set of SFs used in this study.

Category	Title	Definition	Description or formula	Literatures
Derivative spectral features	D_b	Maximum value of 1st derivative within blue edge	Blue edge covers 490–530 nm. D_b is a maximum value of 1st order derivatives within the blue edge of 35 bands	Gong et al. (2002)
	λ_b	Wavelength at D_b	λ_b is wavelength position at D_b	Gong et al. (2002)
	SD_b	Sum of 1st derivative values within blue edge	Defined by sum of 1st order derivative values of 35 bands within the blue edge	Gong et al. (2002)
	D_y	Maximum value of 1st derivative within yellow edge	Yellow edge covers 550–582 nm. D_y is a maximum value of 1st order derivatives within the yellow edge of 28 bands	Gong et al. (2002)
	λ_y	Wavelength at D_y	λ_y is wavelength position at D_y	Gong et al. (2002)
	SD_y	Sum of 1st derivative values within yellow edge	Defined by sum of 1st order derivative values of 28 bands within the yellow edge	Gong et al., (2002)
	D_r	Maximum value of 1st derivative within red edge	Red edge covers 670–737 nm. D_r is a maximum value of 1st order derivatives within the red edge of 61 bands	Gong et al. (2002)
	λ_r	Wavelength at D_r	λ_r is wavelength position at D_r	Gong et al. (2002)
	SD_r	Sum of 1st derivative values within red edge	Defined by sum of 1st order derivative values of 61 bands within the red edge	Gong et al. (2002)
Continuous removal transformed spectral features	Dep	The depth of the feature minimum relative to the hull	In the range of 550–750 nm	Pu et al. (2003, 2004)
	Wid	The full wavelength width at half DEP (nm)	In the range of 550–750 nm	Pu et al. (2003, 2004)
	Area	The area of the absorption feature that is the product of DEP and WID	In the range of 550–750 nm	Pu et al. (2003, 2004)
Hyperspectral vegetation indices	NBNDVI	Narrow-band normalised difference vegetation index	$(R_{850} - R_{680}) / (R_{850} + R_{680})$	Thenkabail et al. (2000)
	NRI	Nitrogen reflectance index	$(R_{570} - R_{670}) / (R_{570} + R_{670})$	Filella et al. (1995)
	TVI	Triangular vegetation index	$0.5[120(R_{750} - R_{550}) - 200(R_{670} - R_{550})]$	Broge and Leblanc (2001)
	PRI	Photochemical/Physiological Reflectance Index	$(R_{531} - R_{570}) / (R_{531} + R_{570})$	Gamon et al. (1992)
	PhRI	The Physiological Reflectance Index	$(R_{550} - R_{531}) / (R_{550} + R_{531})$	Gamon et al. (1992)
	CARI	Chlorophyll absorption ratio index	$([(a670 + R_{670} + b)] / (a^2 + 1)^{1/2}) \times (R_{700} / R_{670})$ $a = (R_{700} - R_{550}) / 150$, $b = R_{550} - (a \times 550)$	Kim et al. (1994)
	TCARI	The transformed chlorophyll absorption and reflectance index	$3[(R_{700} - R_{670}) - 0.2(R_{700} - R_{550})(R_{700} / R_{670})]$	Haboudane et al. (2004)
	MCARI	Modified chlorophyll absorption ratio index	$[(R_{701} - R_{671}) - 0.2(R_{701} - R_{549})] / (R_{701} / R_{671})$	Daughtry et al. (2000)
	RVSI	Red-Edge Vegetation Stress Index	$[(R_{712} + R_{752}) / 2] - R_{732}$	Merton and Huntington (1999)
	PSRI	Plant Senescence Reflectance Index	$(R_{680} - R_{500}) / R_{750}$	Merzlyak et al. (1999)
	ARI	Anthocyanin Reflectance Index	$ARI = (R_{550})^{-1} - (R_{700})^{-1}$	Gitelson et al. (2001)
Broad band spectral features	R_G	Reflectance of green band	Within the range from 520 to 600 nm	(Referred to RSR of Landsat-5 TM)
	R_R	Reflectance of red band	Within the range from 620 to 690 nm	(Referred to RSR of Landsat-5 TM)
	R_{NIR}	Reflectance of near-infrared band	Within the range from 760 to 960 nm	(Referred to RSR of Landsat-5 TM)
	SR	Simple ratio	R_{NIR} / R_R	Baret and Guyot (1991)
	NDVI	Normalized difference vegetation index	$(R_{NIR} - R_R) / (R_{NIR} + R_R)$	Rouse et al. (1973)
	MSR	Modified simple ratio	$(R_{NIR} / R_R - 1) / ((R_{NIR} / R_R)^{0.5} + 1)$	Chen (1996)
	GNDVI	Green normalized difference vegetation index	$(R_{NIR} - R_G) / (R_{NIR} + R_G)$	Gitelson et al. (1996)
	RDVI	Re-normalized difference vegetation index	$(R_{NIR} - R_R) / (R_{NIR} + R_R)^{0.5}$	Roujean and Breon (1995)
NLI	Non-linear vegetation index	$(R_{NIR}^2 - R_R) / (R_{NIR}^2 + R_R)$	Goel and Qi (1994)	

2.4. Regression analysis of SFs with disease severity

Correlation analysis was carried out to examine the sensitivity of each SF to disease severity of powdery mildew. The sensitivity of SFs could be described by the absolute coefficient of correlation (R) between SFs and DI. The higher the absolute R , the stronger the sensitivity of the SF. Based on the sensitivity analysis of SFs, multivariate linear regression (MLR) analysis and partial least square regression (PLSR) analysis were applied and compared for developing multivariate models in estimating DI of powdery mildew. Two measures, the coefficient of determination (R^2) and the relative

root mean square error (RMSE), were used to evaluate the performance of MLR and PLSR models. The relative RMSE is the RMSE divided by the mean of observations. The formula of RMSE is:

$$RMSE = \sqrt{\frac{\sum_{i=1}^n (y_{est,i} - y_{obs,i})^2}{n}} \tag{5}$$

where n is the sample size (in this study, $n = 114$); y_{est} is the estimate of DI; y_{obs} is the DI observation. To avoid a phenomenon of over-fitting in simulating the two regression models, a leave-one-out cross validation approach, called “cross validation approach”,

was adopted to assess the performance of the regression models based on Seymour (1993). To get an estimated DI for a sample, all the other 113 samples ($114 - 1 = 113$ samples) were used to construct a PLSR or MLR model, which was then applied to estimate the DI for the leave-out sample. After a full rotation, a total of 114 DI estimates could be obtained. In addition, the estimates from the model that was fitted by using all 114 samples were also presented in the result section, called “training approach”, in order to differentiate it from the “cross validation approach”.

2.5. Discriminant analysis of disease levels

Before conducting discriminant analysis of disease levels, a two-sample difference *t*-test was conducted to assess the ability of the 32 SFs in separating the three health levels: normal, slightly-damaged and heavily-damaged leaves. Based on the discriminating power of the SFs, the Fisher linear discriminate analysis (FLDA) was applied to establish optimal discriminant models (McLachlan, 2004). Using the same method as the regression analysis, both the training approach and the leave-one-out cross validation approach were utilized to evaluate identifying each sample into one of the three health levels. In addition, due to the inherent ability of the cross validation approach in eliminating the over-fitting phenomenon, it was also used to assess the generation of optimal discriminant models. Finally, overall accuracy (OAA), average accuracy (AA), producer's accuracy, user's accuracy, and *kappa* coefficient were calculated from confusion matrices to evaluate the accuracies of the discriminant analysis. In this study, both MLR and FLDA analyses were implemented in SPSS 19.0 while the PLSR was run by using SAS PLS procedure (SAS 9.2).

3. Results

3.1. Spectral curves of powdery mildew

Fig. 2 illustrates curves of raw reflectances, first-derivative spectra, and reflectance ratios of slightly-damaged ($3\% < \text{lesion portion} < 30\%$) and heavily-damaged (lesion portion $> 30\%$) leaf spectra to normal spectrum (by averaging all the measurements from normal leaves and leaves with a lesion portion $< 3\%$). From Fig. 2a and c, it is easy to see that the spectral difference between normal and slightly-damaged leaves is much smaller than that between normal and heavily-damaged leaves especially in the visible region. In general, compared to normal leaves, raw reflectances of diseased leaves exhibit a significant increase in the visible spectral region from 520 to 720 nm while in the NIR region, such a difference between the raw reflectances is insignificant with a slight decrease of the diseased leaf spectra. The differences of the first derivative spectra (Fig. 2b) between normal, slight-damaged and heavy-damaged leaves are noticeable in the regions from 510 to 530 nm and from 690 to 740 nm, which locate in the green edge and red edge regions. The “blue shifting” phenomenon of red edge positions for the diseased leaves in Fig. 2b is significant. In this case, it does confirm that the technique of extracting red edge optical parameters from hyperspectral data can be used to diagnose a plant's health level (Miller et al., 1991; Baret et al., 1994).

3.2. Regression analysis

Table 2 summarizes the results of correlation analysis between each of the 32 SFs and DIs of the 114 samples. It turns out that 29 SFs significantly correlate with DI ($p\text{-value} < 0.05$). Of them, six SFs have an absolute *R* value over 0.8. They are GNDVI, Wid, MCARI, R_G , SD_b and CARI; 18 SFs have an absolute *R* value over 0.7; and 20 SFs have an absolute *R* value over 0.6. It is interesting to observe that

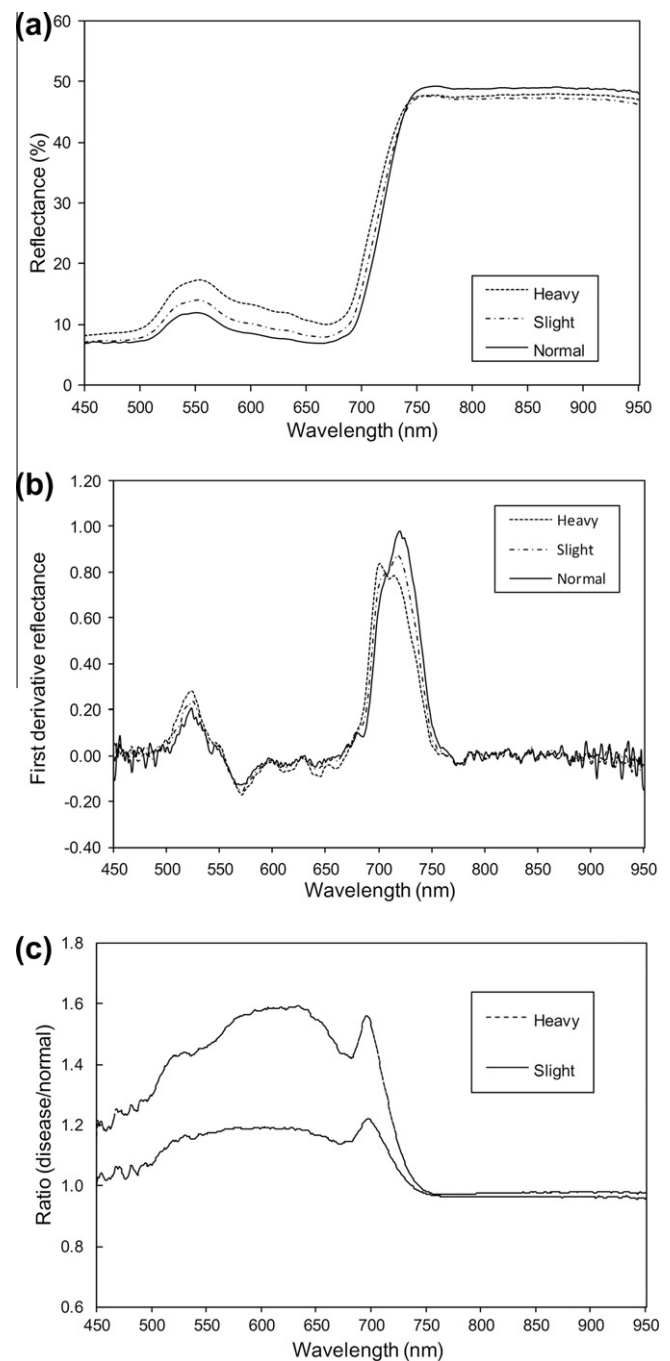


Fig. 2. Curves of raw reflectances, first derivative spectra and reflectance ratios of diseased leaf spectra to normal spectrum. (a) Raw reflectance curves of normal, slightly-damaged ($3\% < \text{lesion portion} < 30\%$) and heavily-damaged (lesion portion $> 30\%$); (b) first derivative spectral curves of normal and diseased leaves; (c) reflectance ratio curves of slightly-damaged and heavily-damaged leaf spectra to normal spectrum.

the broad band SFs perform well in the correlation analysis with the sample DI values in this particular study, eight out of nine SFs achieving an absolute *R* over 0.6.

In order to establish the regression models to estimate the DI value, all 32 SFs were used to create the PLSR model. The relative RMSE values were used to judge how many components should be retained in the PLSR model. Based on a cross validation result, the model composed of seven components yielded the smallest relative RMSE. Therefore, this PLSR model was adopted to estimate the DI value. Correspondingly, the MLR model with the best seven

Table 2
Summary of correlation analysis between SFs and DI ($n = 114$).

Ranking	SFs	R	R^2	p -Value	Ranking	SFs	R	R^2	p -Value
1	GNDVI	-0.889	0.790	0.000	17	SR	-0.728	0.530	0.000
2	Wid	-0.872	0.760	0.000	18	R_R	0.720	0.518	0.000
3	MCARI	0.858	0.736	0.000	19	SD_r	-0.645	0.416	0.000
4	R_G	0.855	0.731	0.000	20	PSRI	0.631	0.398	0.000
5	SD_b	0.827	0.684	0.000	21	SD_y	-0.573	0.328	0.000
6	CARI	0.825	0.681	0.000	22	PRI	-0.565	0.319	0.000
7	D_y	0.784	0.615	0.000	23	PHRI	0.509	0.259	0.000
8	NLI	-0.781	0.610	0.000	24	NRI	0.457	0.209	0.001
9	λ_r	-0.768	0.590	0.000	25	Dep	-0.454	0.206	0.002
10	Area	-0.768	0.590	0.000	26	ARI	0.454	0.206	0.003
11	RDVI	-0.767	0.588	0.000	27	D_r	-0.441	0.194	0.003
12	D_b	0.766	0.587	0.000	28	λ_y	-0.343	0.118	0.003
13	NDVI	-0.762	0.581	0.000	29	R_{NIR}	-0.237	0.056	0.026
14	MSR	-0.739	0.546	0.000	30	λ_b	-0.111	0.012	0.484
15	NBNDVI	-0.735	0.540	0.000	31	RVSI	0.061	0.004	0.701
16	TCARI	0.731	0.534	0.000	32	TVI	-0.052	0.003	0.745

R represents the coefficient of correlation; R^2 represents the coefficient of determination, and all the SFs were ranked by R^2 ; p -value is the probability of accept the null hypothesis.

Table 3
Summary of accuracies of regression models for DI estimation ($n = 114$).

Statistics	PLSR		MLR	
	Training approach	Cross validation approach	Training approach	Cross validation approach
R^2	0.86	0.80	0.81	0.64
Relative RMSE	0.18	0.23	0.23	0.32

SFs (by making MLR and PLSR have the same dimensions) was constructed as well. The R^2 and the relative RMSE values, produced by both PLSR and MLR models using both training approach and cross validation approach were summarized in Table 3. The accuracies of the PLSR model were consistently higher than those of the MLR model. The degree of over-fitting can be explicitly illustrated by using a cross validation approach because in each estimation process, the training sample and test sample are separated. In Table 3, it is obvious that for PLSR model, the values of R^2 and RMSE are better than those of MLR, regardless of whether the training approach or cross validation approach was used. In Fig. 3, with the cross validation approach, the scattering points between estimated DIs and measured DIs for PLSR are more closely distributed along the diagonal line (1:1 dash line) than those for MLR, indicating that PLSR has produced a relatively smaller residual error than MLR. Therefore, it is feasible to draw the conclusion that PLSR can provide more accurate estimation of DI than MLR.

3.3. Discrimination analysis

Other than estimating the DI value in a continuous manner by regression analysis, we also attempted to determine the disease severity levels of leaves in a discrete manner by discrimination analysis. Table 4 summarizes the ability of the 32 SFs in separating normal, slightly-damaged and heavily-damaged samples, evaluated by a p -value of the Independent t -test in SPSS. The rankings of all SFs that are given in Table 4 can be interpreted as their sensitivity to the disease severity levels. The rankings of the 32 SFs appear to be generally consistent with the pattern in Table 2. However, some slight differences still exist, e.g., the GNDVI was ranked 1st in Table 2, whereas it was ranked 2nd in Table 4. These subtle differences might be associated with the different analysis methods (regression and discrimination) and the different data presentation forms of the disease severity (continuous and discrete). As shown in Table 4, based on the p -value, there are seven

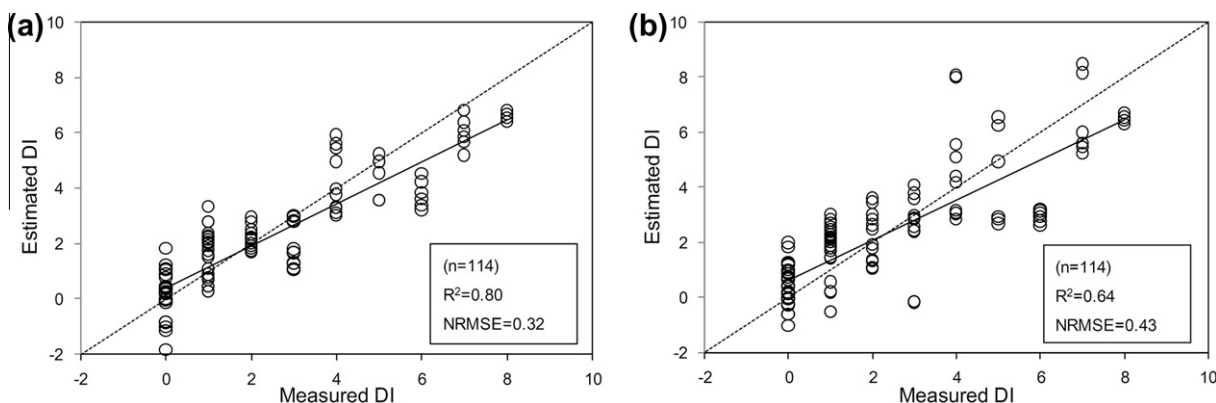


Fig. 3. Scatter plots between measured DI and estimated DI using cross validation approach. (a) PLSR model based on the seven components; (b) MLR model based on the seven best SFs.

Table 4
Summary of independent *t*-test of 32 SFs (*n* = 114).

Ranking	SFs	Significance (<i>p</i> -value)			Ranking	SFs	Significance (<i>p</i> -value)		
		Normal vs. slight	Slight vs. heavy	Normal vs. heavy			Normal vs. slight	Slight vs. heavy	Normal vs. heavy
1	MCARI	***	***	***	17	NDVI		***	***
2	GNDVI	***	***	***	18	RDVI		***	***
3	CARI	***	***	***	19	R_R		***	***
4	SD_b	***	***	***	20	SD_y	***		***
5	R_G	***	***	***	21	NLI		***	***
6	D_b	***	***	***	22	PhRI	**		***
7	Wid	***	***	***	23	D_f	***		***
8	D_y	**	***	***	24	SD_f		**	***
9	λ_f	***	**	***	25	NRI	***		**
10	TCARI	***	*	***	26	RVSI	***		*
11	PSRI	***	*	***	27	PRI		**	*
12	Area	*	***	***	28	Dep			*
13	SR		***	***	29	TVI	*		
14	MSR		***	***	30	λ_y			
15	ARI	***		***	31	λ_b			
16	NBNDVI		***	***	32	R_{NIR}			

* Mean difference is significant at 0.950 confidence level.
 ** Mean difference is significant at 0.990 confidence level.
 *** Mean difference is significant at 0.999 confidence level.

SFs that are significant at 0.999 confidence level for all three pairs, and 12 SFs that are significant at 0.950 confidence level. For the remaining SFs, they exhibit a significant mean difference in at least one pair, except for λ_y , λ_b and R_{NIR} , which fail to show any significant differences in all three pairs.

For those SFs with high sensitivity to leaf powdery mildew, models for identifying normal, slightly-damaged and heavily-damaged leaves were developed using the Fisher linear discriminate analysis (FLDA). To establish a discriminate analysis (DA) model with the highest discriminating power, an important question is how many spectral features should be included in the model. Based on this consideration, prior to FLDA, we conducted a feature selection process as shown in Fig. 4. Although the variation trend of the AA curve turned out to be monotonous when using the training approach, there is a knee point at seven (SFs) based on the result of the cross validation approach (Fig. 4), where the AA reaches the highest value in this particular test. The AA value decreasing after seven variables might be attributed to an over-fitting problem. It could be also considered as redundant information preserved in those variables after seven. Based on this result, the best seven SFs (referring to the ranking order in Table 4, including five hyperspectral SFs and two broad-band SFs) were retained for developing

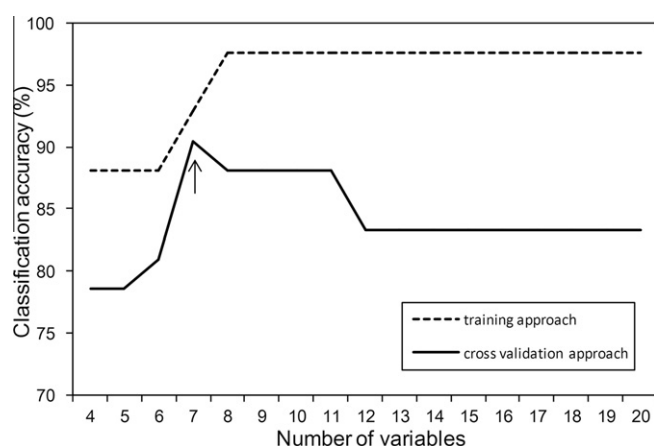


Fig. 4. Variation of classification accuracy with number of variables for both all-fitted approach and cross validation approach. The classification method employed is the Fisher linear discriminate analysis (FLDA).

the discriminating model. In addition, the performance of the model that was constructed by the best seven broad-band SFs (referring to the ranking order in Table 4 for broad-band SFs only) was also examined. The means and standard deviations of the best seven SFs and the best seven broad-band SFs were presented in Fig. 5. It is obvious that the spectral differences of the best seven SFs between normal, slightly-damaged and heavily-damaged leaves are more significant than those of the best seven broad-band SFs. This implies that hyperspectral data would be more powerful in discriminating the three health levels than multispectral data.

The coefficients of the best seven SFs (optimal-model) and the best seven broad-band SFs (broad-band-model) were listed in Table 5. In the broad-band-model, the coefficients for both R_R and MSR are zero. The classification results with both training approach and cross validation approach were listed in two confusion matrices for the optimal-model (Table 6) and two confusion matrices for the broad-band-model (Table 7). By comparing several accuracy indices in Tables 6 and 7, it is easy to see that the classification results of the three health levels produced by the optimal-model are better than those produced by the broad-band-model. This is due to relatively high spectral differences of the seven best SFs between the three health levels (Fig. 5). However, the broad-band-model can also yield an acceptable accuracy, although its classification accuracy is not as high as that of the optimal model. In general, whether using the training approach or the cross validation approach, both models are able to generate relatively high accuracies of classification for the three health levels. When focusing on individual health levels' discriminant results, it is noticeable that higher producer's and user's accuracies (>0.9) were achieved for the heavily-damaged class with both models compared to the other two health levels. The latter has around 80–90% accuracies by using the optimal-model and around 70–80% accuracies by using the broad-band-model.

4. Discussion

The spectral response of powdery mildew was first observed by Lorenzen and Jensen (1989). In their study, they found that the disease severity of leaves become explicit with the passage of time after they were inoculated. The longer the time after the plants were inoculated, the more serious symptoms would become. However, to measure different severity degrees of powdery mildew on plant leaves from different developing stages of the disease would

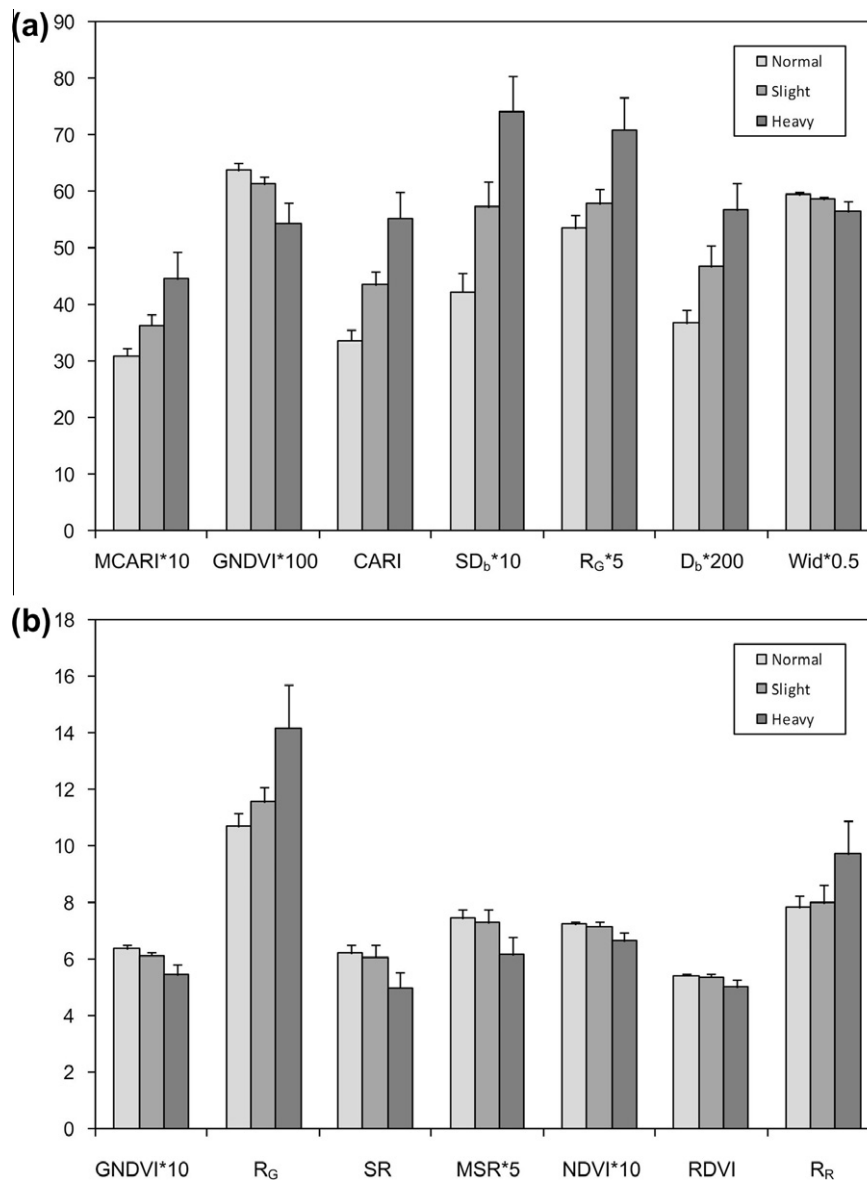


Fig. 5. Means (bar) and standard deviations (short line) of selected SFs in normal, slightly-damaged and heavily-damaged classes. (a) The best seven SFs; (b) the best seven broad-band SFs. Some SFs were adjusted by multiplying a coefficient to enhance the comparability among them.

Table 5
A summary of discriminant coefficients in FLDA models ($n = 114$).

Spectral feature	Seven best SFs			Spectral feature	Seven broad-band SFs		
	Normal	Slight	Heavy		Normal	Slight	Heavy
D_b	-2733	-2793	-2753	R_G	1452	1452	1452
SD_b	317	322	320	SR	-566	-567	-567
Wid	239	243	245	NDVI	88,200	88,210	88,200
R_G	408	399	399	GNDVI	294	284	269
GNDVI	3034	2807	2564	RDVI	-4579	-4578	-4577
CARI	25	25	25	R_R	0	0	0
MCARI	-392	-360	-354	MSR	0	0	0
(Constant)	-17,620	-17,870	-18,050	(Constant)	-23,460	-23,460	-23,450

inevitably bring about a mixture phenomenon of phonological change signals, with the disease induced signals of the plant leaves. To deal with this imperfection, the present study attempted to determine the severity level of a leaf directly based on the cover percentage of pustule on a leaf, which could thus exclude the phonological impact.

According to existing studies, the change of reflectance that occurs in diseased leaves is driven by the breakdown of chlorophyll pigments and subsequent changes in the carotenoids, anthocyanins and xanthophylls pigments (Gamon et al., 1992; Penuelas et al., 1994; Devadas et al., 2009), as well as the breakdown of the cell structure. These processes could lead to corresponding

Table 6

Confusion matrices created based on both all-fitted approach and cross validation approach for the optimal-model.

		Reference				U's a. (%)	OAA	AA	κ
		Normal	Slight	Heavy	Sum				
<i>All-fitted approach</i>									
Classified	Normal	30	5	0	35	85.71	0.92	0.93	0.88
	Slight	4	43	0	47	91.49			
	Heavy	0	0	32	32	100.00			
	Sum	34	48	32	114				
	P.'s a. (%)	88.24	89.58	100.00					
<i>Cross validation approach</i>									
Classified	Normal	30	6	0	36	83.33	0.89	0.90	0.84
	Slight	4	41	1	46	89.13			
	Heavy	0	1	31	32	96.88			
	Sum	34	48	32	114				
	P.'s a. (%)	88.24	85.42	96.88					

Note: OAA is overall accuracy; AA is average accuracy; P.'s a. represents producer's accuracy; U.'s a. represents user's accuracy.

Table 7

Confusion matrices based on both all-fitted approach and cross validation approach for the broad-band-model.

		Reference				U's a. (%)	OAA	AA	κ
		Normal	Slight	Heavy	Sum				
<i>All-fitted approach</i>									
Classified	Normal	29	7	0	36	80.56	0.88	0.88	0.81
	Slight	5	41	2	48	85.42			
	Heavy	0	0	30	30	100.00			
	Sum	34	48	32	114				
	P.'s a. (%)	85.29	85.42	93.75					
<i>Cross validation approach</i>									
Classified	Normal	27	9	0	36	75.00	0.83	0.84	0.75
	Slight	7	38	2	47	80.85			
	Heavy	0	1	30	31	96.77			
	Sum	34	48	32	114				
	P.'s a. (%)	79.41	79.17	93.75					

Note: See Table 6 for explanations of the accuracy index abbreviations in the table.

changes of reflectance in the visible and NIR spectral regions in general, particularly around 470, 670 (absorption of chlorophyll), 550 (green peak), and 730 nm (red edge) (West et al., 2003; Sankaran et al., 2010). In our study, it is obvious that the spectral reflectances at all these particular positions respond significantly to powdery mildew (Fig. 2). However, the spectral responses turn to be weak and invisible after 730 nm in the NIR region (reflectance ratios are around 1.0), which confirms the results reported by other researchers (see Fig. 2 in Lorenzen and Jensen (1989)). Theoretically, the breakdown of the cell structure is assumed to reduce the reflectance in the NIR region. In addition to the breakdown of pigments and the destruction of cell structures, the powder on the leaf's surface also plays an important role in altering the leaf's spectrum. The white color of pustules could increase the reflectances in both visible and NIR regions, which might offset the influence from the breaking of cell structures, and make the reflectance change in the NIR region insignificant. The same impact from pustule color was also observed by Devadas et al. (2009).

As mentioned in Sections 3.2 and 3.3, it is encouraging to find that most SFs in Table 1 are sensitive to the powdery mildew, particularly for those broad-band SFs, which exhibit great potential in detecting powdery mildew (Tables 2 and 4) with multispectral data. For regression analysis, with the same number of components (variables for MLR model) as inputs, the PLSR model outperformed MLR model according to the accuracy indices created with the cross validation approach. A great advantage of PLSR over a traditional regression method is its capability in not only lowering dimensionality of the raw data but retaining majority of variance contained in the raw data as well. For example, in the present study, 32 variables were reduced to seven components that were

actually combinations of those raw variables. Such a transformation facilitates the concentration of principal information of independent variables and also helps eliminate the correlations between components (Li et al., 2002; Faber and Rajkó, 2007). Since the MLR model just used the seven selected variables (without considering using information from remaining variables), it is easy to understand why it performed much poorer than the PLSR in this particular case. Therefore, the PLSR method is suggested to be applied for estimating the disease severity with leaf spectral measurements although it is more difficult to interpret the PLSR's result than MLR's.

In addition to the regression analysis, the discrimination analysis also yielded satisfactory results in this study (Tables 6 and 7). However, the successful rates of classification were not equal among the different health levels. The heavily-damaged leaves could be accurately identified using the cross validation approach with both the user's and producer's accuracy over 90% for both of the discriminating models, the optimal-model and the broad-band-model. In comparison to the heavily-damaged samples, the successful rates of the other two levels were around 70–80% using the cross validation approach, which indicated that there existed a certain degree of confusion between them. To explore the cause for the different success rates among the three health levels, mean difference tests of the pigment contents between any two levels (pairs) of the three levels were conducted using an independent *t*-test in SPSS. The test results were summarized in Table 8. Per the table, significant differences were found for Chla, Chlb, Chla+b and Car contents between normal and heavily-damaged samples and between slightly-damaged and heavily-damaged samples. However, for the pair of normal and slightly-damaged samples,

Table 8
A summary of independent *t*-test of pigments between the three healthy levels.

Samples	Chla	Chlb	Chla+b	Car	Car/Chla+b
Normal vs. slight					*
Normal vs. heavy	***	***	***	**	*
Slight vs. heavy	**	***	***	***	

* Mean difference is significant at 0.950 confidence level.

** Mean difference is significant at 0.990 confidence level.

*** Mean difference is significant at 0.999 confidence level; "slight" indicates using slightly-damaged samples, and "heavy" indicates using heavily-damaged samples.

the differences of those pigments were not significant at 0.95 confidence level. Such a pattern of pigments differences between the three health levels was in a good agreement with the pattern revealed by the spectral discrimination analysis, which could be viewed as a physical basis of the spectral discrepancies among different health levels. In addition, compared to the normal and slightly-damaged samples, the higher cover percentage of pustule on leaves of heavily-damaged samples would increase the spectral separability between them due to the significant difference of the leaf color. Therefore, to effectively make use of the remote sensing techniques for detecting powdery mildew in practice, it is suggested that a high accuracy could be guaranteed only if the cover percentage of pustule on leaves is over 30%. As for different model forms, although the accuracy of the broad-band-model was slightly lower than that of the optimal-model, such an accuracy was still acceptable, with the OAA of 0.83 and the κ coefficient of 0.75. Unlike some plant diseases detected by using only relatively narrow band data (Huang et al., 2007; Devadas et al., 2009), the relatively broad band and strong spectral response of powdery mildew allow us to detect or discriminate the disease by using commonly used multispectral remote sensing systems, which could thus lower the cost of the operation significantly (West et al., 2003; Hahn, 2009; Sankaran et al., 2010). For example, with routine multispectral Landsat TM products, it is possible to map the spatial distribution of powdery mildew in a winter wheat field in the season of the disease occurrence.

5. Conclusions

The remote detection of powdery mildew infection would be of value for monitoring the disease and offering a direction of fungicide spray tasks. In this study, it was found that the powdery mildew could induce a significant spectral change in both visible and NIR regions, which enables the detection of the disease by remote sensing means. PLSR and FLDA were demonstrated to be efficient in estimating and discriminating the disease severity levels using the selected spectral features. It is encouraging that those selected broad-band spectral features exhibited great potential in detecting powdery mildew at a leaf level with commonly used multispectral remote sensing data, such as Landsat TM data.

However, in field conditions, it remains challenging to upscale the relationship between spectral features and disease severity to canopy level. Apart from the traits on the leaves that are induced by powdery mildew, the leaf architecture, multiple scattering phenomena in canopy reflectance as well as the other possible stressors such as drought and insufficient of nitrogen can also have a certain impact on canopy spectra, which may complicate the relationship between spectral features and disease severity levels. In our further studies, some physically-based models for simulating the radiometric transfer process in the canopy, such as PROSPECT + SAIL, will be incorporated in the up-scaling process. Studies addressing the above questions are necessary in the future.

Acknowledgements

This work was subsidized by the natural science foundation of Beijing city (4122032), the National Natural Science Foundation of China (41071276, 41101395), the National Basic Research Program of China (2011CB311806). The authors are grateful to Mr. Weiguo Li and Mrs. Hong Chang for help of data collection. Thanks also to Ms. Amor Elder, University of South Florida, Tampa, FL for her valuable comments on this paper.

Reference

- Baret, F., Guyot, G., 1991. Potentials and limits of vegetation indices for LAI and APAR assessment. *Remote Sensing of Environment* 35 (2–3), 161–173.
- Baret, F., Vanderbilt, V.C., Steven, M.D., Jacquemoud, S., 1994. Use of spectral analogy to evaluate canopy reflectance sensitivity to leaf optical properties. *Remote Sensing of Environment* 48 (2), 253–260.
- Bravo, C., Moshou, D., West, J., McCartney, A., Ramon, H., 2003. Early disease detection in wheat fields using spectral reflectance. *Biosystems Engineering* 84 (2), 137–145.
- Broge, N.H., Leblanc, E., 2001. Comparing prediction power and stability of broadband and hyperspectral vegetation indices for estimation of green leaf area index and canopy chlorophyll density. *Remote Sensing of Environment* 76 (2), 156–172.
- Cao, X.R., Zhou, Y.L., Duan, X.Y., Cheng, D.F., 2009. Estimation of the effects of powdery mildew on wheat yield and protein content using hyperspectral remote sensing. *Acta Phytophylacica Sinica* 36 (1), 32–36.
- Chen, J.M., 1996. Evaluation of vegetation indices and a modified simple ratio for boreal applications. *Canadian Journal of Remote Sensing* 22 (3), 229–242.
- Christou, P., Twyman, R.M., 2004. The potential of genetically enhanced plants to address food insecurity. *Nutrition Research Reviews* 17, 23–42.
- Daughtry, C.S., Walthall, C.L., Kim, M.S., de Colstoun, E.B., McMurtrey, J.E., 2000. Estimating corn leaf chlorophyll concentration from leaf and canopy reflectance. *Remote Sensing of Environment* 74 (2), 229–239.
- Devadas, R., Lamb, D.W., Simpfendorfer, S., Backhouse, D., 2009. Evaluating ten spectral vegetation indices for identifying rust infection in individual wheat leaves. *Precision Agriculture* 10 (6), 459–470.
- Eichmann, R., Hüchelhoven, R., 2008. Accommodation of powdery mildew fungi in intact plant cells. *Journal of Plant Physiology* 165 (1), 5–18.
- Faber, N.M., Rajkó, R., 2007. How to avoid over-fitting in multivariate calibration—The conventional validation approach and an alternative. *Analytica Chimica Acta* 595 (1–2), 98–106.
- Filella, I., Serrano, L., Serra, J., Penuelas, J., 1995. Evaluating wheat nitrogen status with canopy reflectance indices and discriminant analysis. *Crop Science* 35 (5), 1400–1405.
- Franke, J., Menz, G., 2007. Multi-temporal wheat disease detection by multi-spectral remote sensing. *Precision Agriculture* 8 (3), 161–172.
- Gamon, J.A., Penuelas, J., Field, C.B., 1992. A narrow-waveband spectral index that tracks diurnal changes in photosynthetic efficiency. *Remote Sensing of Environment* 41 (1), 35–44.
- Gitelson, A.A., Kaufman, Y., Merzlyak, M.N., 1996. Use of a green channel in remote sensing of global vegetation from EOS-MODIS. *Remote sensing of Environment* 58 (3), 289–298.
- Gitelson, A.A., Merzlyak, M.N., Chivkunova, O.B., 2001. Optical properties and nondestructive estimation of anthocyanin content in plant leaves. *Photochemistry and Photobiology* 74 (1), 38–45.
- Goel, N.S., Qi, W., 1994. Influences of canopy architecture on relationships between various vegetation indices and LAI and FPAR: A computer simulation. *Remote Sensing Reviews* 10 (4), 309–347.
- Goetz, A.F.H., Vane, G., Solomon, J.E., Rock, B.N., 1985. Imaging spectrometry for earth remote sensing. *Science* 228 (4704), 1147–1153.
- Gong, P., Pu, R., Heald, R.C., 2002. Analysis of in situ hyperspectral data for nutrient estimation of giant sequoia. *International Journal of Remote Sensing* 23 (9), 1827–1850.
- Gooding, M.J., Smith, S.P., Davies, W.P., Kettlewell, P.S., 1994. Effects of late-season applications of propiconazole and tridemorph on disease, senescence, grain development and the breadmaking quality of winter wheat. *Crop Protection* 13 (5), 362–370.
- Graeff, S., Link, J., Claupein, W., 2006. Identification of powdery mildew (*Erysiphe graminis* sp. *tritici*) and take-all disease (*Gaeumannomyces graminis* sp. *tritici*) in wheat (*Triticum aestivum* L.) by means of leaf reflectance measurements. *Central European Journal of Biology* 1 (2), 275–288.
- Haboudane, D., Miller, J.R., Pattery, E., Zarco-Tejad, P.J., Strachan, I.B., 2004. Hyperspectral vegetation indices and novel algorithms for predicting green LAI of crop canopies: Modeling and validation in the context of precision agriculture. *Remote Sensing Environment* 90 (3), 337–352.
- Hahn, F., 2009. Actual pathogen detection: sensors and algorithms - a review. *Algorithms* 2, 301–338.
- Hardwick, N.V., Jenkins, J.E.E., Collins, B., Groves, S.J., 1994. Powdery mildew (*Erysiphe graminis*) on winter wheat: control with fungicides and the effects on yield. *Crop Protection* 13 (2), 93–98.

- Hu, T.Z., Li, H.J., Xie, C.J., You, M.S., Yang, Z.M., Sun, Q.X., Liu, Z.Y., 2008. Molecular mapping and chromosomal location of powdery mildew resistance gene in wheat cultivar tangmai. *Acta Agronomica Sinica* 34 (7), 1193–1198.
- Huang, W.J., David, W.L., Niu, Z., Zhang, Y.J., Liu, L.Y., Wang, J.H., 2007. Identification of yellow rust in wheat using in-situ spectral reflectance measurements and airborne hyperspectral imaging. *Precision Agriculture* 8 (4–5), 187–197.
- Jones, C.D., Jones, J.B., Lee, W.S., 2010. Diagnosis of bacterial spot of tomato using spectral signatures. *Computers and Electronics in Agriculture* 74 (2), 329–335.
- Jørgensen, L.N., Olesen, J.E., 2002. Fungicide treatments affect yield and moisture content of grain and straw in winter wheat. *Crop Protection* 21 (10), 1023–1032.
- Kim, M.S., Daughtry, C.S.T., Chappelle, E.W., McMurtrey, J.E. 1994. The use of high spectral resolution bands for estimating absorbed photosynthetically active radiation (APAR). In *Proceedings of the 6th International Symposium on Physical Measurements and Signatures in Remote Sensing*. France. Val d'Isere. pp. 299–306.
- Li, B., Morris, J., Martin, E.B., 2002. Model selection for partial least squares regression. *Chemometrics and Intelligent Laboratory Systems* 64 (1), 79–89.
- Lichtenthaler, H.K., 1987. Chlorophylls and carotenoids: pigments of photosynthetic biomembranes. *Methods in Enzymology* 148, 350–382.
- Liu, Z.Y., Wu, H.F., Huang, J.F., 2010. Application of neural networks to discriminate fungal infection levels in rice panicles using hyperspectral reflectance and principal components analysis. *Computers and Electronics in Agriculture* 72 (2), 99–106.
- Lorenzen, B., Jensen, A., 1989. Changes in leaf spectral properties induced in barley by cereal powdery mildew. *Remote Sensing of Environment* 27 (2), 201–209.
- Luedeling, E., Hale, A., Zhang, M., Bentley, W.J., Dharmasri, L.C., 2009. Remote sensing of spider mite damage in California peach orchards. *International Journal of Applied Earth Observation and Geoinformation* 11 (4), 244–255.
- McLachlan, G.J., 2004. *Discriminant Analysis and Statistical Pattern Recognition*. Wiley Interscience.
- Merton, R., Huntington, J., 1999. Early simulation of the ARIES-1 satellite sensor for multi-temporal vegetation research derived from AVIRIS. In: *Summaries of the Eight JPL Airborne Earth Science Workshop*. Pasadena, CA: JPL, Publication. pp. 299–307.
- Merzlyak, M.N., Gitelson, A.A., Chivkunova, O.B., Rakitin, V.Y., 1999. Non-destructive optical detection of pigment changes during leaf senescence and fruit ripening. *Physiologia Plantarum* 106 (1), 135–141.
- Miller, J.R., Wu, J., Boyer, M.G., Belanger, M., Hare, E.W., 1991. Season patterns in leaf reflectance red edge characteristics. *International Journal of Remote Sensing* 12 (7), 1509–1523.
- Moshou, D., Bravo, C., West, J., Wahlen, S., McCartney, A., Ramon, H., 2004. Automatic detection of 'yellow rust' in wheat using reflectance measurements and neural networks. *Computers and Electronics in Agriculture* 44 (3), 173–188.
- Nofal, M.A., Haggag, W.M., 2006. Integrated management of powdery mildew of mango in Egypt. *Crop Protection* 25 (5), 480–486.
- Olsen, M., Rasmussen, S., Nischwitz, C., 2003. Effect of powdery mildew of pecan shucks on nut weight and quality and relevance to fungicide application. *Crop Protection* 22 (4), 679–682.
- Penuelas, J., Gamon, J.A., Fredeen, A.L., Merino, J., Field, C.B., 1994. Reflectance indices associated with physiological changes in nitrogen- and water-limited sunflower leaves. *Remote sensing of Environment* 48 (2), 135–146.
- Pu, R., Foschi, L., Gong, P., 2004. Spectral feature analysis for assessment of water status and health level in coast live oak (*Quercus agrifolia*) leaves. *International Journal of Remote Sensing* 25 (20), 4267–4286.
- Pu, R., Ge, S., Kelly, N.M., Gong, P., 2003. Spectral absorption features as indicators of water status in coast live oak (*Quercus agrifolia*) leaves. *International Journal of Remote Sensing* 24 (9), 1799–1810.
- Qin, Z.H., Zhang, M.H., 2005. Detection of rice sheath blight for in-season disease management using multispectral remote sensing. *International Journal of Applied Earth Observation and Geoinformation* 7 (2), 115–128.
- Reuveni, R., Reuveni, M., 1998. Foliar-fertilizer therapy—a concept in integrated pest management. *Crop Protection* 17 (2), 111–118.
- Rémus-Borel, W., Menzies, J.G., Bélanger, R.R., 2005. Silicon induces antifungal compounds in powdery mildew-infected wheat. *Physiological and Molecular Plant Pathology* 66 (3), 108–115.
- Roujean, J., Breon, F., 1995. Estimating PAR absorbed by vegetation from bidirectional reflectance measurements. *Remote Sensing of Environment* 51 (3), 375–384.
- Rouse, J.W., Haas, R.H., Schell, J.A., Deering, D.W., 1973. Monitoring vegetation systems in the Great Plains with ERTS. *Proc. Third ERTS Symposium* 1, 48–62.
- Rumpf, T., Mahlein, A.K., Steiner, U., Oerke, E.C., Dehne, H.W., Plümer, L., 2010. Early detection and classification of plant diseases with Support Vector Machines based on hyperspectral reflectance. *Computers and Electronics in Agriculture* 74 (1), 91–99.
- Sankaran, S., Mishra, A., Ehsani, R., Davis, C., 2010. A review of advanced techniques for detecting plant diseases. *Computers and Electronics in Agriculture* 72 (1), 1–13.
- Seymour, G., 1993. *Predictive inference. An introduction*. Chapman & Hall, New York.
- Sharma, A.K., Sharma, R.K., Srinivasa Babu, K., 2004. Effect of planting options and irrigation schedules on development of powdery mildew and yield of wheat in the North Western plains of India. *Crop Protection* 23 (3), 249–253.
- Strange, R.N., Scott, P.R., 2005. Plant disease: a threat to global food security. *Annual Review of Phytopathology* 40, 83–116.
- Thenkabail, P.S., Smith, R.B., De Pauw, E., 2000. Hyperspectral vegetation indices and their relationships with agricultural crop characteristics. *Remote Sensing of Environment* 71 (2), 158–182.
- West, J.S., Bravo, C., Oberti, R., Lemaire, D., Moshou, D., McCartney, H.A., 2003. The potential of optical canopy measurement for targeted control of field crop diseases. *Annual Review of Phytopathology* 41, 593–614.
- Wright, D.P., Baldwin, B.C., Shephard, M.C., Scholes, J.D., 1995. Source-sink relationships in wheat leaves infected with powdery mildew II. Changes in the regulation of the Calvin cycle. *Physiological and Molecular Plant Pathology* 47 (4), 255–267.
- Yang, C.M., Cheng, C.H., Chen, R.K., 2007. Changes in spectral characteristics of rice canopy infested with brown planthopper and leafhopper. *Crop Science* 47 (1), 329–335.
- Zhao, C.J., Huang, M.Y., Huang, W.J., Liu, L.Y., Wang, J.H., 2004. Analysis of winter wheat stripe rust characteristic spectrum and establishing of inversion models. *IGARSS 6 (20–24)*, 4318–4320.